On 3D flow pattern behind a wall-mounted circular cylinder of finite-length

Cite as: AIP Conference Proceedings **2323**, 030002 (2021); https://doi.org/10.1063/5.0041449
Published Online: 08 March 2021

Václav Uruba, and Pavel Procházka

On 3D Flow Pattern Behind a Wall-Mounted Circular Cylinder of Finite-Length

Václav Uruba[1, 2, a)] and Pavel Procházka[1, b)]

[1]*Institute of Thermomechanics of the Czech Academy of Sciences, Dolejškova 5, 182 00 Praha 8, Czech Republic*
[2]*Faculty of Mechanical Engineering, Department of Power System Engineering, Universitní 8, Plzeň, Czech Republic*
[a)]Corresponding author: uruba@it.cas.cz
[b)]prochap@it.cas.cz

Abstract. The wake behind a wall-mounted finite-length circular cylinder of the aspect ratio 2 stuck out of a wall was studied experimentally using stereo PIV technique. The cylinder was mounted normal to a ground plane and it was subjected to a cross-flow with thin boundary layer developed on the wall, the Reynolds number based on inflow velocity and cylinder diameter was 9.7 thousands. The time-averaged velocity and streamwise vorticity fields showed the development of the mean flow structure consisting of the tip vortex pair, the extent of the near-wake recirculation zone with back-flow, the downwash phenomenon and base vortex structures close to the wall.

INTRODUCTION

Infinitely long circular cylinder in cross-flow is one of the canonical cases of flow over a bluff-body. However, every real cylinder is of a limited length, sometimes even with a low aspect ratio (AR) meaning the ratio of its length L to diameter D, mathematically AR = L/D. There are numerous technical applications of the finite-length cylinder, ranging from obstacles in flow parts in turbo-machines to typical architectonic structures including buildings.

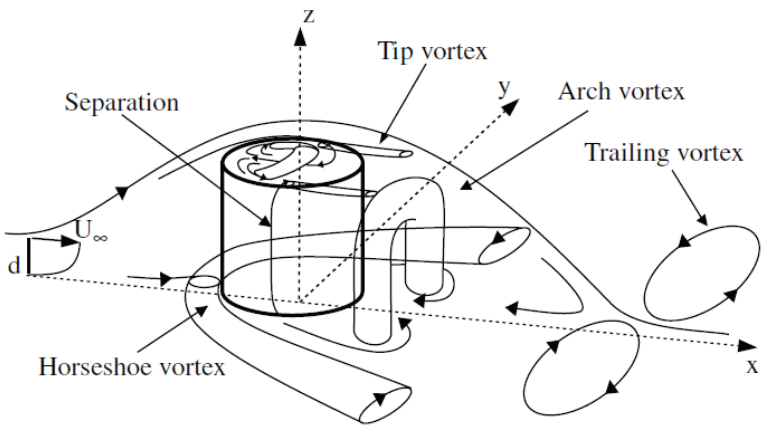

FIGURE 1. Schematic diagram of the time-averaged flow over a truncated cylinder (not to scale) - [8].

In available literature several studies related to the finite-length cylinders in cross-flow could be found [1-9,12-14]. Most of studies are applying mathematical modelling, only a few of them present results of experiments. However the most attention attract the case of a square cylinder, representing a typical building of skyscraper type [1,2,12,14],

19th Conference on Power System Engineering
AIP Conf. Proc. 2323, 030002-1–030002-11; https://doi.org/10.1063/5.0041449
Published by AIP Publishing. 978-0-7354-4067-8/$30.00

only few studies deal with circular cylinder [3-8,13]. As for the aspect ratio, most studies are concentrated on cases characterized by the AR = 5-15, smaller AR is explored seldom. The flow behind the cylinder of the aspect ratio higher than 5 is similar to that of the infinite cylinder with dominating Kármán-Bénárd vortex street (see e.g. [11]), however deformed in a 3D manner and with strong end effects. The shorter cylinders are characterized by qualitatively different flow structure. In paper [6] the critical value of the AR is defined, bellow which the vortex shedding changes from the antisymmetrical Kármán type to the symmetric arch-type. The critical value of the aspect ratio AR_{crit} is reported to be between 2 and 6 (see e.g. [14]). The subcritical case is characterized by parallel vortex shedding in the wake. Then both the tip and base vortices resulted from the projection of the three-dimensional arch-type flow structure in the cross-section plane. The horse-shoe vortex originates in subsequence of the wall-boundary layer – cylinder interaction and trailing (base) vortex is the result of the strong downwash effect. It is worth mentioning that the time-averaged flow structure may not reflect correctly the details of the instantaneous flow structure. The schematic picture is shown in Fig. 1, borrowed from [8].

The presented study is concentrated on the subcritical aspect ratio case resulting in arch-type vortex shedding. Only time-mean structures are to be studied, however a very strong dynamics is detected. Dynamical aspects will be addressed in future publications.

EXPERIMENTAL SETUP

In our case the cylinder of the aspect ratio AR = L/D = 2, length L = 60 mm, diameter D = 30 mm was used. The cylinder is attached to the wall perpendicularly to the flow, see Fig. 2, where the Cartesian coordinate system (x,y,z) is introduced. The Cartesian coordinate system has origin in the center of the cylinder on the wall, x axis is oriented in the flow direction, while the y axis is perpendicular to the flow direction and the cylinder axis. All dimensions are expressed in multiples of the cylinder diameter. The cylinder and the wall (z_r = 0) are in green in Fig. 2. The planes of measurement are perpendicular to flow x_r = constant, there are 15 planes of measurement defined ($x_r = x/D$ = 0.667, 0.833, 1.167, 1.5, 1.833, 2.167, 2.5, 2.833, 3.167, 3.5, 3.833, 5.5, 7.167, 8.833, 10.5), they are in grey. The plane of symmetry (y_r = 0) is in red and the surface plane (y_r = 0.5) in yellow. The surface plane intersects the cylinder surface line on its contour and it is parallel to the plane of symmetry.

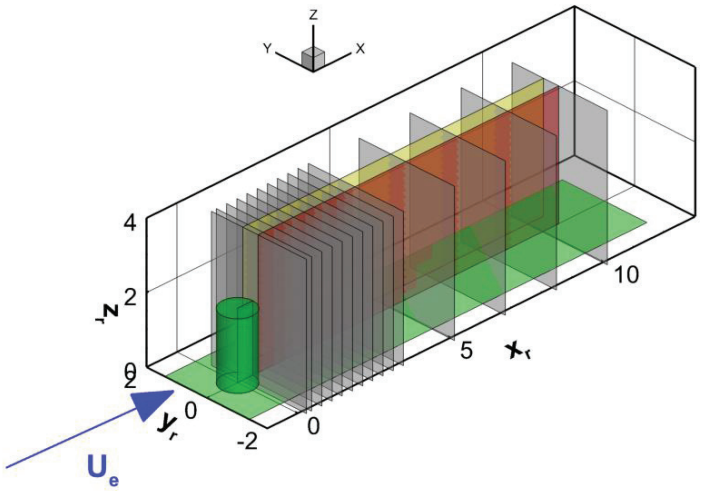

FIGURE 2. Schematics of the experiment.

The test section of the blow-down facility is equipped with impermeable walls. The cross-section of the test section is 250 x 250 mm^2, thus the blockage of the cross-section by the model is less than 3 %. The boundary layer on the walls upstream the cylinder is very thin due to contraction located just upstream, its thickness is about a few millimeters (2-3 mm) as evaluated in preliminary experiments using the hot-wire technique. The in-flow velocity was U_e = 5 m/s, resulting Reynolds number based on cylinder diameter was about 9.7 thousands.

The velocity vector fields were measured using Particle Image Velocimetry (PIV) method. The measurement apparatus consists of laser and 2 CMOS cameras by Dantec Company. The laser is New Wave Pegasus, Nd:YLF double head with wavelength of 527 nm, with maximal frequency 10 kHz and shot energy of 10 mJ (for 1 kHz), thus the corresponding power is 10 W per one head. The 2 cameras VEO 410 with resolution of 1 280 x 800 pixels are able to acquire double snaps with frequency up to 2500 Hz (full resolution) and they use internal memory 16 GB each. The Scheinpflug mounting were used for the cameras lenses to get the focus planes identical with the laser-sheet plane. The stereo-PIV configuration is a standard one described e.g. in [10]. The data were acquired and post-processed using the Dynamic Studio and Tecplot software.

The PIV measurement was performed in the spanwise planes – see Fig. 2. Statistics were evaluated from data acquired with frequency 100 Hz, 1 000 double-snapshots representing 10 s in real time. The Safex generator of particles in the form of oil droplets was used, the mean diameter of the particles was 1 μm as shown in experimental studies by the apparatus supplier.

The stereo PIV method provides all 3 velocity vector components, which were evaluated in each plane of measurement (*yz*). The resolution of the field of interest was 94 x 56 vectors. More detailed description of the experimental setup and procedures could be found in [10].

RESULTS

All results are to be shown in dimensionless form. The geometric dimensions are expressed in multiples of the cylinder diameter D (values of x_r, y_r and z_r respectively) and the velocities in multiples of the inlet velocity U_e. The velocities were subjected to statistical analysis, time-mean values and statistical moments were evaluated. The vorticity is also dimensionless, as it is calculated from dimensionless velocities and distances.

The results are to be shown in streamwise and spanwise planes, and in 3D representation respectively.

Streamwise Planes

First, the velocity distributions in the planes (*xz*) are to be shown. The data is interpolated from the planes of measurement, which are perpendicular to these planes. In Fig. 3 there is mean velocity vectors distribution. The vector-lines are added to recognize better the flow-field structure. The cylinder is shown in black, flow is from left to right.

The color corresponds to the streamwise mean velocity component value. The mean velocity vectors are shown together with the corresponding vector-lines in black. The white line represents the border of back-flow region, which is located just behind the cylinder, attached to it.

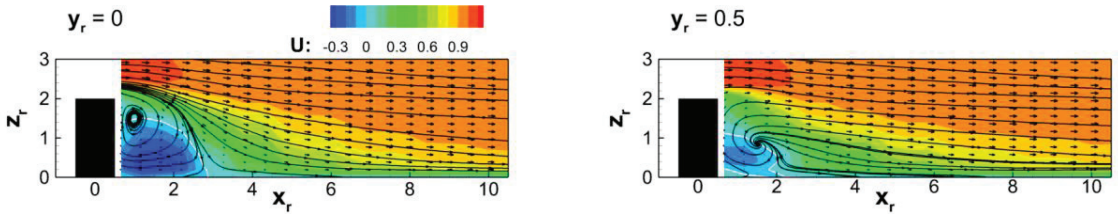

FIGURE 3. Time-mean velocity distribution in the plane of symmetry ($y_r = 0$) on left and surface plane ($y_r = 0.5$) on right.

The vector-lines are backswept towards the wall, which is in position $z = 0$. This is due to the downwash effect of the wake, the fluid from the outer flow-field is pushed towards the wall and the wake is suppressed in the streamwise direction. The vortex, which is located in the plane of symmetry $y_r = 0$ in the position $x_r = 0.9$ and $z_r = 1.5$, is shifted in the surface plane $y_r = 0.5$ to the new position $x_r = 1.57$ and $z_r = 0.8$. Very probably these are the arch vortex intersections (compare with Fig. 1).

Next, the turbulent kinetic energy (TKE) is evaluated from all 3 velocity components to assess the intensity of the flow dynamics. In Fig. 4 the region of increased dynamic activity is shown forming the wake interior in red. The TKE distribution is shown in the plane of symmetry on the left-hand side of the Fig. 4 and the surface plane on the right-hand side.

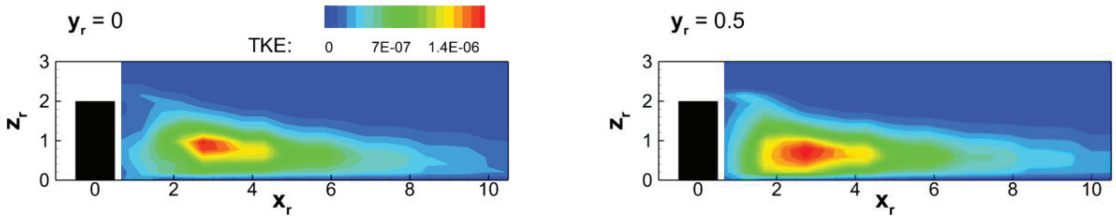

FIGURE 4. Turbulent kinetic energy distribution in the plane of symmetry ($y_r = 0$) on left and surface plane ($y_r = 0.5$) on right.

Decreasing height of the wake in streamwise direction connected with the downwash effect is evident. Maximum of the TKE is located about 3 diameters downstream close to the mid height of the cylinder, however in the surface plane the region of high turbulent activity is much larger than that in the plane of symmetry.

Note the wavy character of the streamwise isolines, this artefact is connected with interpolation between planes of measurement.

Spanwise Planes

Distributions of velocity and vorticity in planes of measurement (yz) is to be shown next. The progress in the streamwise direction will be demonstrated on the mean streamwise velocity component distribution and spanwise mean velocity component topology. The U velocity component distribution is to be shown on the left-hand side together with the back-flow border (line in white). On the right-hand side of each figure the in-plane mean velocity components are depicted in the form of vectors with vector-lines. The color represents streamwise vorticity component, red positive, blue negative. The cylinder silhouette is shown by the broken line.

In Fig. 5, there is the result of analysis in the plane $x_r = 0.83$, this means in the distance 0.33 behind the cylinder rear surface.

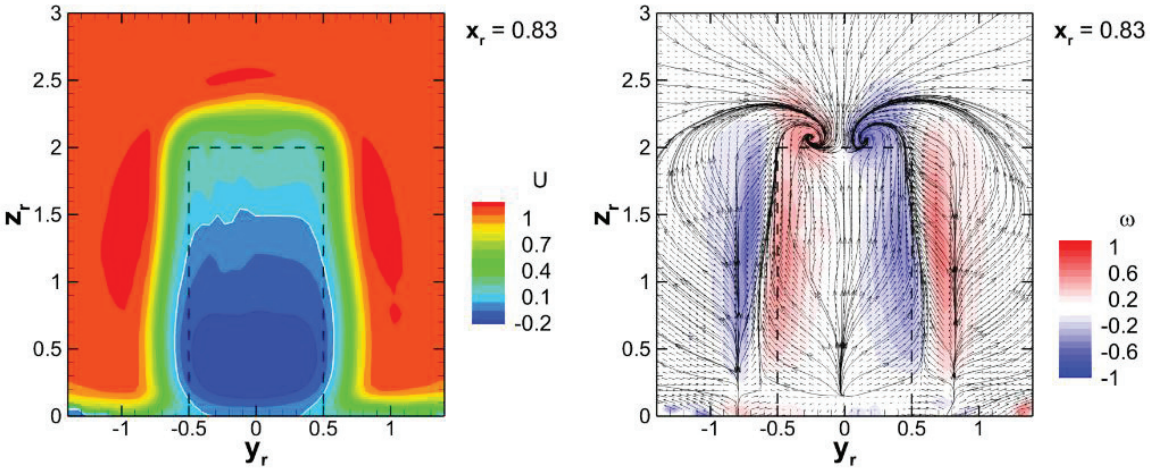

FIGURE 5. Streamwise (left) and spanwise (right) mean velocity components distributions in position $x_r = 0.83$.

In the distributions we could recognize origin of the tip contra-rotating vortices close to the cylinder free end, position $y_r = +\text{-}0.25$, $z_r = 2.05$. The shear regions parallel to the cylinders vertical edges generate high vorticity values, positive and negative. Above the cylinder the downwash effect is visible, while within the cylinders projection the opposite up-wash process is present. There are 3 up-wash regions, one in the center, two on the sides. The back-flow region is behind the cylinder contour, in its lower 2/3. Close to the wake top and sides the overshoot regions with increased velocity are present (deep red spots).

As the boundary layer on the wall upstream the cylinder was very thin, the horseshoe vortex was not detected in our case.

Please note the legends of U and ω, the same legends are valid for results in Figs. 6-12 bellow.

In the following Fig. 6 the plane $x_r = 1.17$ is depicted.

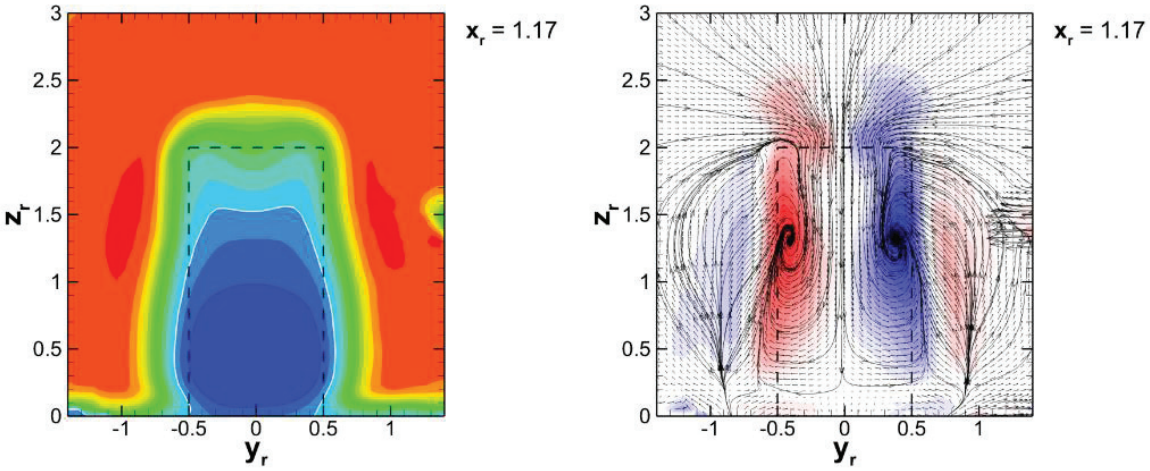

FIGURE 6. Streamwise (left) and spanwise (right) mean velocity components distributions in position $x_r = 1.17$.

The tip contra-rotating vortices are shifted downwards position of about $z_r = 1.3$ and they are stronger. This is the result of the downwash effect. The downwash region penetrates towards the bottom wall in the center and fills the full height of the cylinder near the axis, and up-wash region is split and shifted to sides. The size and topology of the back-flow region is more or less the same. The two saddle regions parallel with the cylinder side contours in Figs. 5 and 6 could be prints of the arch vortex – see Fig. 1

The following plane of measurement $x_r = 1.5$ is shown in Fig. 7.

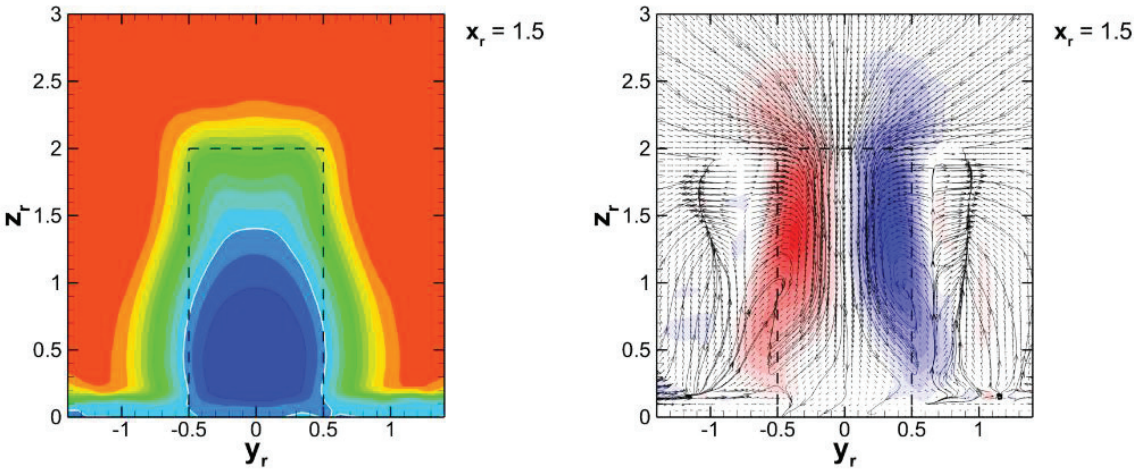

FIGURE 7. Streamwise (left) and spanwise (right) mean velocity components distributions in position $x_r = 1.5$.

Here, the tip vortices disappear completely, only strong shear regions marked by positive and negative vorticity value is seen close to the cylinders sides' projection. The up-wash regions are still on sides and the downwash region stays in the middle. The back-flow region is even smaller.

The next plane of measurement $x_r = 2.17$ is in Fig. 8.

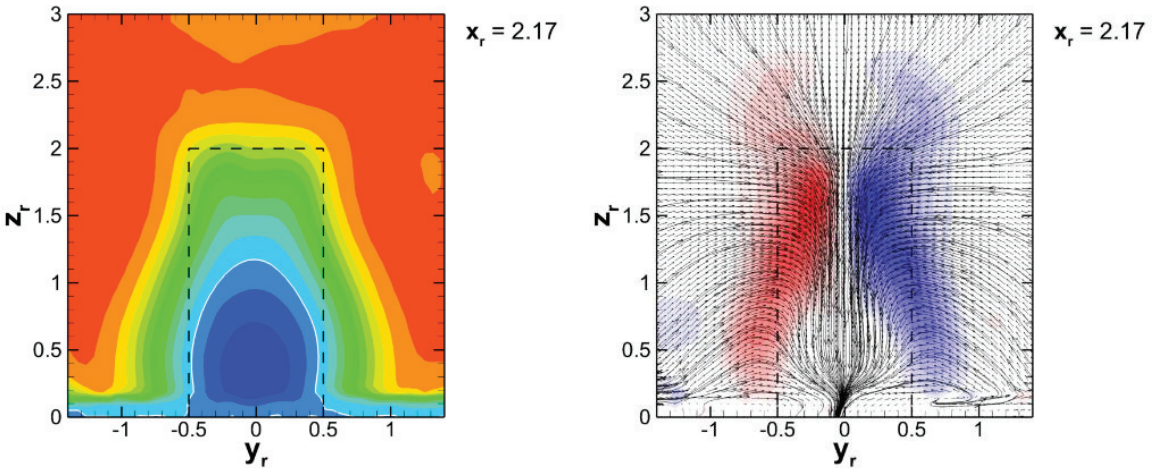

FIGURE 8. Streamwise (left) and spanwise (right) mean velocity components distributions in position $x_r = 2.17$.

The side up-wash effect is much weaker here, the shear regions parallel to the cylinder axis indicated by strong vorticity are shifted towards the cylinder center. Further downstream the up-wash effect getting stronger forming the trailing vortices – see Fig. 9.

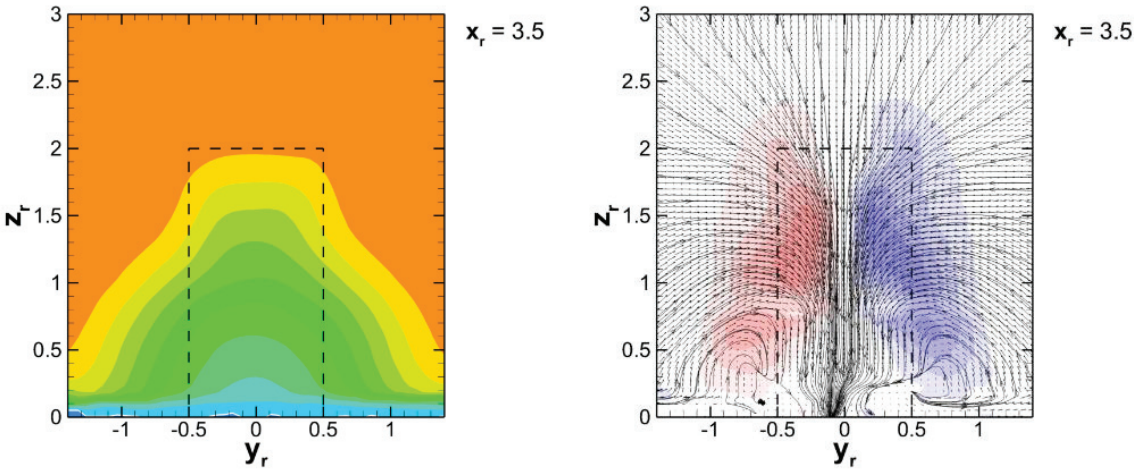

FIGURE 9. Streamwise (left) and spanwise (right) mean velocity components distributions in position $x_r = 3.5$.

The trailing vortices cores nuclei are formed in position $x_r = 3.5$, in coordinates $y_r = +\text{-}0.8$, $z_r = 0.3$. The back-flow region disappeared completely here.

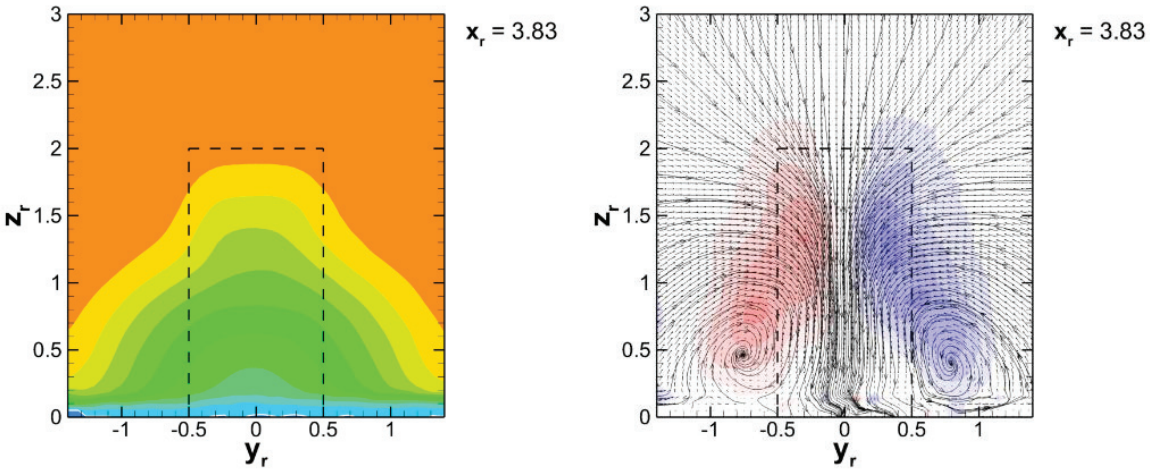

FIGURE 10. Streamwise (left) and spanwise mean velocity components distributions in position $x_r = 3.83$.

In the next position $x_r = 3.83$, see Fig. 10, the trailing vortex pair is already well developed. The downwash in the center and up-wash on sides becomes a dominant flow-field feature again. Further development of the trailing base vortices is demonstrated in Figs. 11 and 12 demonstrating gradual wake development in positions $x_r = 5.5$ and 10.5 respectively.

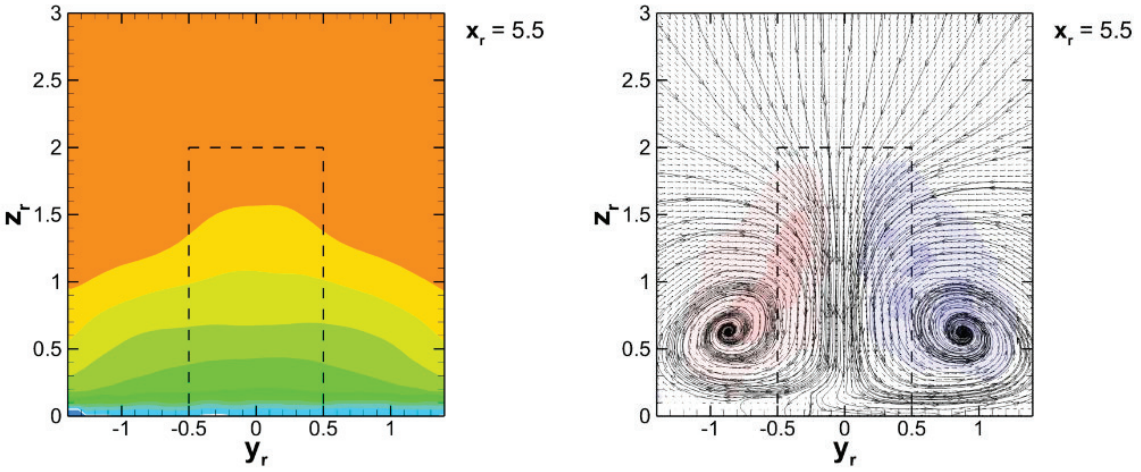

FIGURE 11. Streamwise (left) and spanwise (right) mean velocity components distributions in position $x_r = 5.5$.

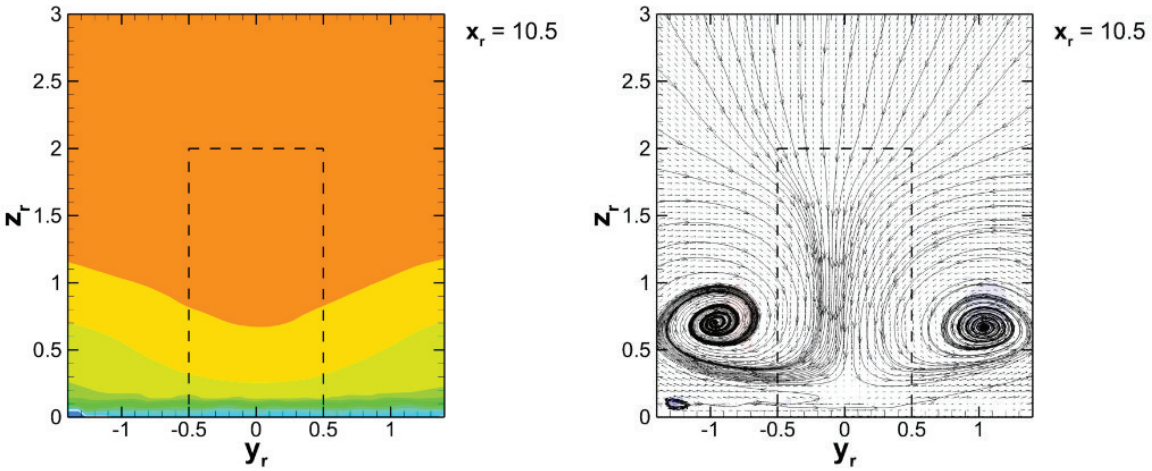

FIGURE 12. Streamwise (left) and spanwise (right) mean velocity components distributions in position $x_r = 10.5$.

The base trailing vortices are well-developed and they are shifted towards the sides. They are distinct, however weaker than upstream (vorticity value weakens). The other mean-time structures are suppressed completely.

The wake is split into 2 side parts and starts to disappear in the center – see Fig. 12 on the left with minimum in the center.

3D Distributions

The 3D topologies of the selected time-mean quantities distributions in space will be presented now.

The back-flow zone topology is in Fig. 13. The surface (in light blue) is located in the wake behind the cylinder, maximal height is about 2/3 of the cylinder length, disappearing on position about $x_r = 3$ on the flow axis.

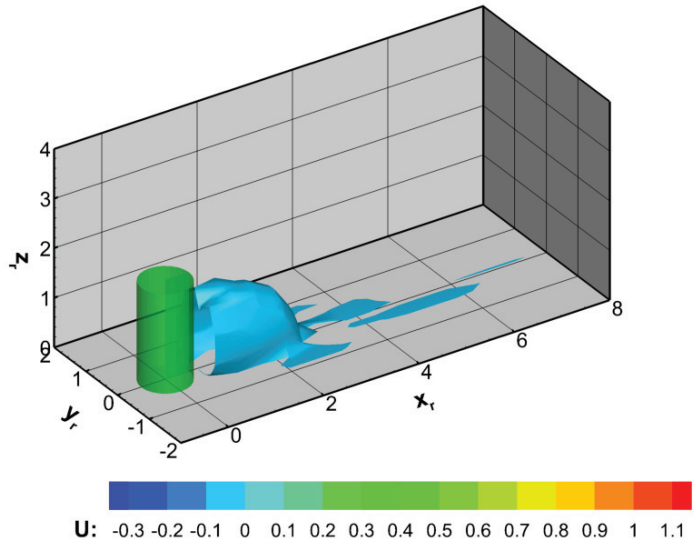

FIGURE 13. Zero streamwise mean velocity component topology, $U = 0$.

The high fluctuating activity zone topology in the wake is in Fig. 14.

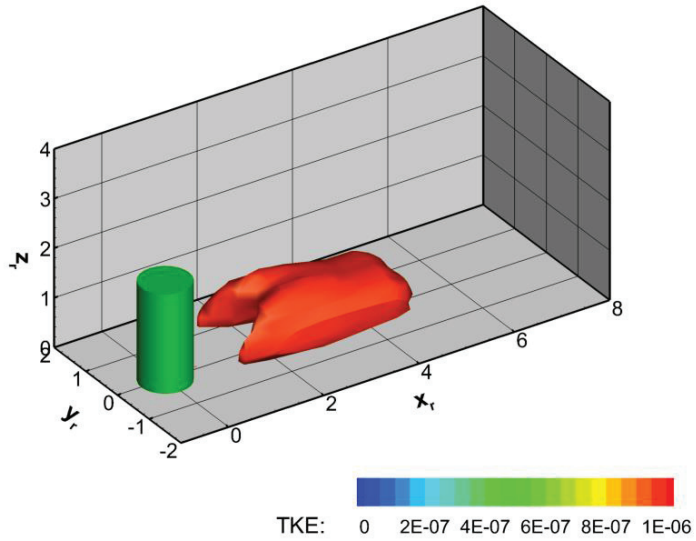

FIGURE 14. High TKE topology, TKE = 1e-6.

The TKE iso-surface split structure with 2 peaks close to the cylinder side contours merging together in the cylinders mid-height. Compare with the TKE distributions in the streamwise planes Fig. 4. The value TKE of 1e-6 (it is dimensionless) represents about 70% of the peak TKE value in the region.

The last iso-surface represents the mean streamwise vorticity component. The positive (red) and negative (blue) mean vorticity streamwise component topology is in Fig. 15 in the form of iso-surfaces representing about 1/3 of the vorticity peak value.

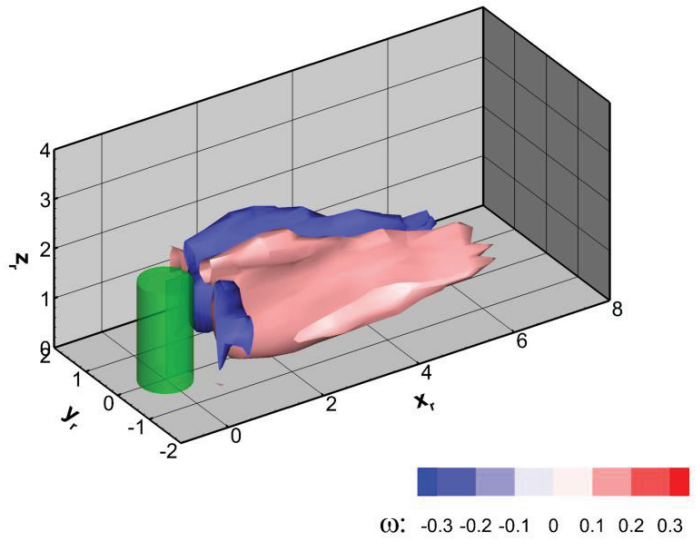

FIGURE 15. Positive and negative streamwise vorticity component, $\omega = +\text{-}0.1$.

The main structures are located behind the cylinder sides contours located symmetrically with the corresponding orientation, positive on the right and negative on the left (looking in the stream direction). The secondary small structures are more on sides with opposite orientation. Confirm the *z*-planes Figs. 5 and 6, maximal vorticity value in the region is $\omega = +\text{-}1$. The main vorticity region belongs to the tip vortex and strong shear along the cylinder. The secondary vorticity is generated by the arch vortex.

The detailed view on tip vortices is shown in Fig. 16.

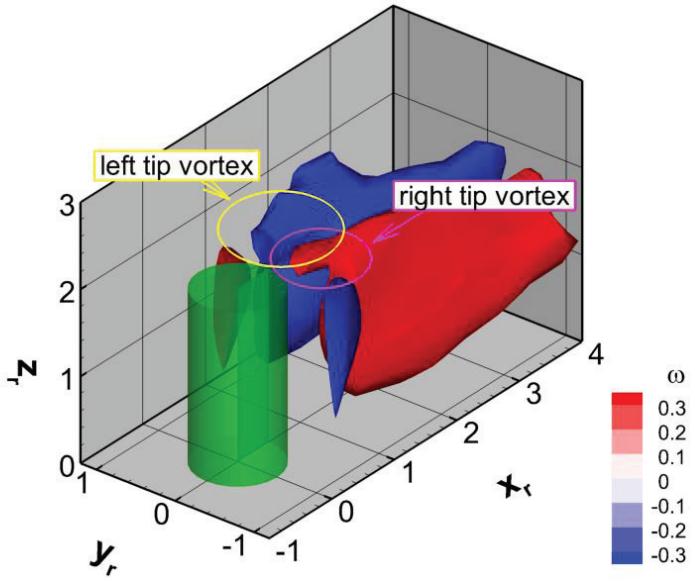

FIGURE 16. Positive and negative streamwise vorticity component, $\omega = +\text{-}0.3$, detail of the tip vortices.

The tip vortex is forms by elongated vorticity region oriented in streamwise direction just above the cylinder upper end. The right tip vortex is positive (anticlockwise, in red), while the left tip vortex has negative orientation (clockwise, in blue). The huge region of high vorticity below the tip vortices belongs to strong shear regions, compare with Figs. 5-8.

CONCLUSIONS

The mean-time structure of the wake behind a wall-mounted circular cylinder of the aspect ratio 2 has been shown. The mean velocity and vorticity fields have been evaluated and depicted.

The horseshoe vortex was not detected, as the boundary layer upstream the cylinder is very thin. The tip vortex couple is clearly detected in close wake, for $x_r < 1.5$. The base trailing vortex appears due to downwash effect in the wake center and up-wash on sides. It was created in the position $x_r = 3.5$. The arch vortex was detected in the wake very close, just behind the cylinder in the distance $x_r \approx 1$.

The time-mean averaged structures are the starting point for the subsequent analysis of the flow dynamics.

ACKNOWLEDGMENT

This work was supported by the Grant Agency of the Czech Republic, project No. 17-01088S, 19-04695S and 19-02288J.

REFERENCES

1. Ch. Amor, J.M. Pérez, P.Schlatter, R.Vinuesa, and S. Le Clainche, Soft computing techniques to analyze the turbulent wake of a wall-mounted square cylinder, *Advances in Intelligent Systems and Computing*, pp 577–86, 2019
2. Ch. Amor, J.Pérez, P.Schlatter, R.Vinuesa, S.Le Clainche, Modeling the turbulent wake behind a wall-mounted square cylinder. *Logic Journal of IGPL*. 1-11. 10.1093/OUP. (2020)
3. S.Le Clainche, J.M. Pérez and J.M.Vega, Spatio-temporal flow structures in the threedimensional wake of a circular cylinder, *Fluid Dyn. Res.* 50 (2018) 051406 (19pp)
4. C.R. Johnston, D.J.Wilson, A Vortex Pair Model for Plume Downwash into Stack Wakes, *Atmospheric Environment*, Vol. 31, No.1, pp. 13-30 (1997)

5. S. Krajnovic, Flow around a tall finite cylinder explored by large eddy simulation, *J. Fluid Mech*., Vol. 676, 2011, pp. 294-317
6. C. Norberg, An experimental investigation of the flow around a circular cylinder: influence of aspect ratio, *J. Fluid Mech.* (1994), vol. 258, pp. 287-316
7. G.Palau-Salvador, T.Stoesser, J.Frohlich, M.Kappler, & W.Rodi, 2010 Large eddy simulations and experiments of flow around finite-height cylinders. *Flow Turbul. Combust.* 84, pp239–275.
8. R.J. Pattenden, S.R. Turnock, X. Zhang, Measurements of the flow over a low-aspect ratio cylinder mounted on a ground plate. *Exp. Fluids* 39, 10–21 (2005)
9. P. Procházka and V. Uruba, Reynolds Number Effect on Velocity Field and on Coherent Structures behind a Cylinder, *AIP Conf. Proc*. 2118, 030037-1–030037-4; (2019) 38th Meeting of Departments of Fluid Mechanics and Thermodynamics; Wellness and Kongress Hotel CHOPOK Liptovsky Mikulas; Slovakia; 19 June 2019 through 21 June 2019; Code 149090
10. P. Procházka, V. Uruba, V. Skála, Evolution of vortical structures behind an inclined flat plate, *MATEC Web of Conferences* 168 (2018) Article number 05003
11. A. Roshko, On the development of turbulent wakes from vortex streets. *NACA Rep. 1191*, pp.801-825 (1955)
12. A. K. Saha, Unsteady flow past a finite square cylinder mounted on a wall at low Reynolds number, *Comput. Fluids*, Vol. 88, 2013, pp. 599-615
13. D. Sumner, J.L. Heseltine, O.J.P. Dansereau, Wake structure of a finite circular cylinder of small aspect ratio, *Experiments in Fluids* 37 (2004) 720–730
14. H.F. Wang, Y. Zhou, The finite-length square cylinder near wake, J. Fluid Mech. (2009), vol. 638, pp. 453–490